E1-2007-4

J. Fedorišin[a,1], S. Vokál[a,b,2]

SEARCH FOR THE RING-LIKE STRUCTURES IN THE EMISSION OF SECONDARY PARTICLES IN CENTRAL ^{197}Au COLLISIONS WITH EMULSION NUCLEI AT 11.6A GeV/c

Submitted to «Journal of Physics G»

[1] E-mail: fedorisi@kosice.upjs.sk
[2] E-mail: vokal@sunhe.jinr.ru
[a] University of P. J. Šafárik, Košice, Slovakia
[b] Joint Institute for Nuclear Research, Dubna

Федоришин Я., Вокал С. E1-2007-4

Поиск кольцевых структур в эмиссии вторичных частиц в центральных соударениях ядер ^{197}Au с ядрами эмульсии при 11,6A ГэВ/c

С целью поиска кольцевых структур, которые могут служить указанием на образование черенковских глюонов или ударных волн Маха в возбужденной ядерной материи, методом непрерывного вейвлет-анализа исследованы угловые спектры вторичных релятивистских частиц, рожденных в Au+Em-соударениях при импульсе 11,6A ГэВ/c. Анализ основан на предположении, что эти эффекты могут проявиться как повышенный выход частиц при определенных псевдобыстротах. Кроме того, ожидается равномерное азимутальное угловое распределение таких частиц. В результате при точности шкал до 0,5 были обнаружены нерегулярности в вейвлетных спектрах, которые интерпретируются нами как псевдобыстроты приоритетного испускания групп частиц. Проведенный анализ азимутальной структуры этих нерегулярностей показал, что они не являются кольцевыми структурами.

Работа выполнена в Лаборатории высоких энергий им. В. И. Векслера и А. М. Балдина ОИЯИ.

Препринт Объединенного института ядерных исследований. Дубна, 2007

Fedorišin J., Vokál S. E1-2007-4

Search for the Ring-Like Structures in the Emission of Secondary Particles in Central ^{197}Au Collisions with Emulsion Nuclei at 11.6A GeV/c

Angular spectra of the relativistic secondary particles produced in Au+Em nuclear collisions at 11.6A GeV/c are analyzed by the method of continuous wavelet transform in order to search for the ring-like structures which could indicate either the production of Cherenkov gluons or the occurrence of Mach shock waves in excited nuclear matter. The analysis is based on the assumption that the presence of the above-mentioned effects would be manifested by excess of particles at some characteristic pseudorapidities. In addition, the involved particles are expected to be azimuthally uniformly distributed. The irregularities are revealed in the wavelet pseudorapidity spectra in the scale pseudorapidity region up to 0.5. These irregularities are interpreted as the preferred pseudorapidities of groups of emitted particles. The performed study of the azimuthal structure of the above-mentioned pseudorapidity irregularities suggests that they are not related to the sought ring-like structures.

The investigation has been performed at the Veksler and Baldin Laboratory of High Energies, JINR.

Preprint of the Joint Institute for Nuclear Research. Dubna, 2007

INTRODUCTION

Cherenkov electromagnetic radiation is a well-known phenomenon in high-energy physics. It is emitted when a charged particle passes through an insulator at a speed v greater than the speed of light c_{medium} in that medium. Produced photons which are in phase with each other can constructively interfere to form a cone centered along the direction of moving particle. The cone is described by opening angle θ defined as:

$$\cos\theta = \frac{c_{\mathrm{medium}}}{v} = \frac{c}{nv}, \tag{1}$$

where n is the refractive index of the medium. As was proposed in [1, 2], a partonic jet traversing nuclear medium could become the source of conical gluon radiation similar to that of Cherenkov photon radiation. The predicted effect is again described by formula (1), where v represents the velocity of triggering particle (parton) and c_{medium} is the typical speed of gluons in nuclear matter. The necessary conditions to observe such an effect could be attained in the collisions of nuclei at high energies when an impinging nuclei can be looked upon as a bunches of partons traversing the nuclear medium of target nucleons. The emission of Cherenkov gluons would eventually form the ring-like structures of produced particles in the plane perpendicular to the direction of original parton as shown in Fig. 1.

The alternative hypothesis clarifying the occurrence of ring-like structures in the angular spectra of secondary particles is the creation of Mach shock waves in nuclear medium [3]. This idea is now largely discussed mainly in the context of RHIC experiments [4]. The mechanism is analogous to that of the radiation of Cherenkov photons or gluons except that the speed c_{medium} in formula (1) would stand for the speed of sound in nuclear matter.

Under the assumption the direction of initial parton coincides with the direction of impinging beam, the plane in Fig. 1 will coincide with azimuthal plane. Therefore, the distributions of both the azimuthal and polar angles of secondary particles must be analyzed simultaneously to detect the ring-like structures. Instead of polar angle a pseudorapidity defined as

$$\eta = -\ln\left(\tan\frac{\theta}{2}\right) \tag{2}$$

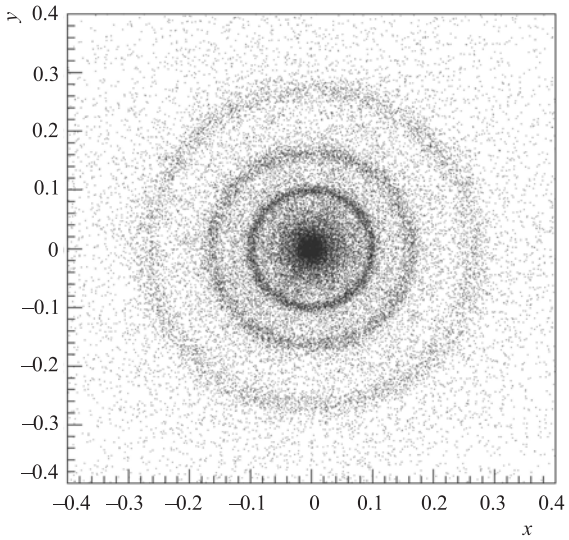

Fig. 1. Illustrative picture of particles emitted in the form of ring-like structures — the MC simulation

can be used if the analysis is restricted only to relativistic particles. Anyway, the occurrence of ring-like structures would be manifested by the two main signatures in the spectra of secondary particles:

- peaks or bumps in θ (or η) distribution;
- approximately uniform azimuthal distributions (at certain scales).

The second item reflects the possibility of the emission of only a few Cherenkov gluons resulting in the production of only several sparse minijets which would lead to large fluctuations in azimuthal spectra mainly at small scales. The uniformity would appear at large scales reflecting the azimuthal distribution of minijets seen indirectly through the groups of particles originating from them.

1. EXPERIMENT

The experimental data used in this analysis was obtained at AGS accelerator located at BNL. The stacks of NIKFI BR-2 nuclear photoemulsion were exposed to the beam of ^{197}Au nuclei at 11.6A GeV/c momenta. The photoemulsion technique is capable to detect the tracks of charged particles along with their azimuthal angles ϕ and polar angles θ measured with respect to the beam direction. More detailed description of the employed experimental method can be found in [5].

The experimental data set consists of 1071 inelastic min-bias events. For the purpose of this analysis only the s-particles defined as single-charged particles

with a velocity $\beta = v/c \geqslant 0.7$ are taken into account. The reason for that is that s-particles consist mainly of particles created in the collisions and, thus, they could include the particles resulted from the searched effects as well. Simultaneosly the multiplicities of s-particles can be adopted as a criterion for the centrality of the collisions.

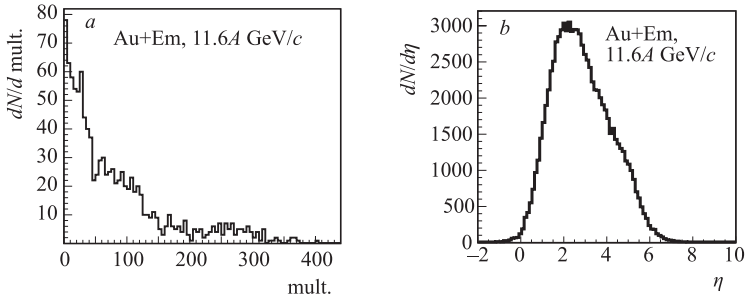

Fig. 2. Distributions of multiplicities of s-particles produced in Au+Em interactions

The highest multiplicities of s-particles are above 300 which can be seen in Fig. 2, a.

Fig. 2, b presents the pseudorapidity spectrum of all s-particles produced in all Au+Em collisions.

2. METHOD

The wavelet method employed to survey the angular spectra of produced particles provides handy mathematical tools to determine simultaneously positions and widths of irregularities which can be interpreted as particle collective flows. The another great advantage is that unlike Fourier analysis where only two basis functions exist, the wavelet analysis have an infinite set of possible basis functions. The wavelet basis should be chosen according to the properties of expected signals in order to ensure more direct and transparent access to information. In general, the continuous wavelet transform of function *f(x)* has the form:

$$W_\Psi(a,b)f = \frac{1}{\sqrt{C_\Psi}} \int_{-\infty}^{\infty} f(x)\Psi_{a,b}(x)dx, \tag{3}$$

where *x* is a studied quantity and C_Ψ is a normalizing constant. The functions

$$\Psi_{a,b}(x) = a^{-1/2}\Psi\left(\frac{x-b}{a}\right) \tag{4}$$

are shifted and/or dilated derivations of mother wavelet function $\Psi(x)$ characterized by translation parameter *b* and dilation parameter or scale *a*. The coefficients $W_\Psi(a,b)$ can be interpreted as contributions (amplitudes) of wavelets $\Psi_{a,b}$ to spectrum *f(x)*.

Since in our case the analysis is restricted only to relativistic particles, it is quite justified to deal with pseudorapidities η rather than with polar angles θ. The distribution of pseudorapidities can be expressed as [6]:

$$f(\eta) = \frac{dn}{d\eta} = \frac{1}{N}\sum_{i=1}^{N}\delta(\eta - \eta_i), \tag{5}$$

where *N* is the number of s-particles in a studied data sample and η_i is pseudorapidity of i-th particle. Data sample can mean either a few events or one single event or only a part of event. The wavelet transform of the function (5) takes on the form [7]:

$$W_\Psi(a,b)f = \frac{1}{N}\sum_{i=1}^{N} a^{-1/2}\Psi\left(\frac{\eta_i - b}{a}\right). \tag{6}$$

Wavelet pseudorapidity spectrum at some scale is thus the sum of wavelets representing individual particles. Wavelet coefficients $W_\Psi(a,b)$ reflect the probability to observe particle at some pseudorapidity *b* and scale *a*. Therefore, the wavelet coefficients are helpful to estimate prevailing scales and preferred pseudorapidities.

In our analysis we use the second derivative $g_2 = (1-x^2)e^{-x^2/2}$ of Gaussian function (also known as Mexican hat, shown in Fig. 3) as mother wavelet since the signals of approximattely Gaussian-like shape are anticipated. The additional

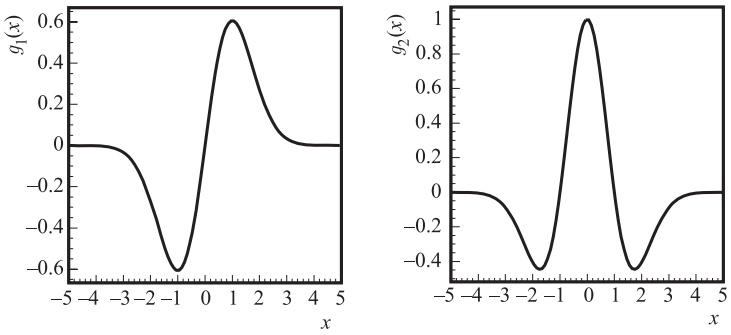

Fig. 3. The first two derivatives of Gaussian function

reason is that g_2 wavelet constitutes the best compromise reaching a satisfactory resolution in both the scale and the pseudorapidity domains.

3. ANALYSIS OF WAVELET PSEUDORAPIDITY DISTRIBUTIONS

The application of the wavelet transform to the pseudorapidity distribution of all s-particles (shown in Fig. 2, b) allows one to investigate its behaviour at various scales. This approach basically means that only the global features of the studied events are extracted but this is quite sufficient at the very first step. Wavelet g_2 pseudorapidity spectra for all the studied Au events at the three different scales a are presented in Fig. 4.

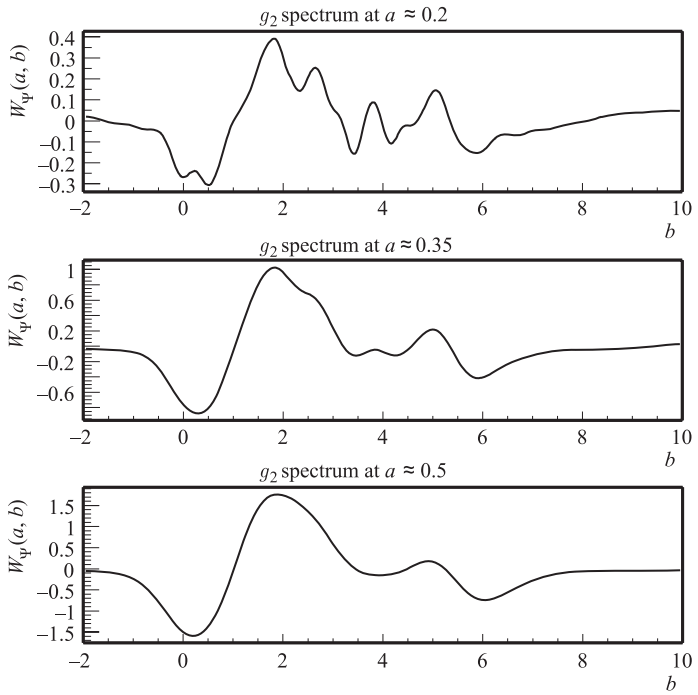

Fig. 4. Wavelet g_2 pseudorapidity spectra of all the studied Au events seen at the three different scales a

The maximums in the spectra in Fig. 4 are related to preferred pseudorapidities of groups of secondary particles. The size of groups is indicated by the scales a. At the finest scales only the small particle groups are observed while at the coarse scales the large particle collective flows are clearly discernible. The number of particles included in separate groups follows from the size of areas corresponding to the local maximums. The size of each area is indicated by its width and height of the maximum. The particles can be roughly assorted to the three main groups: 1. the target fragmentation region at low pseudorapidities,

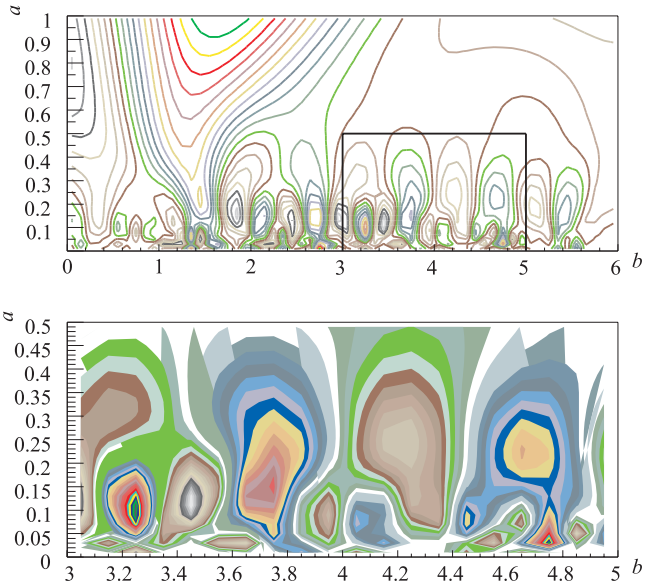

Fig. 5. Wavelet pseudorapidity spectrum of the random Au event with multiplicity ≈ 100. The lower picture is the rectangle area from the upper picture zoomed only to show better some interesting details

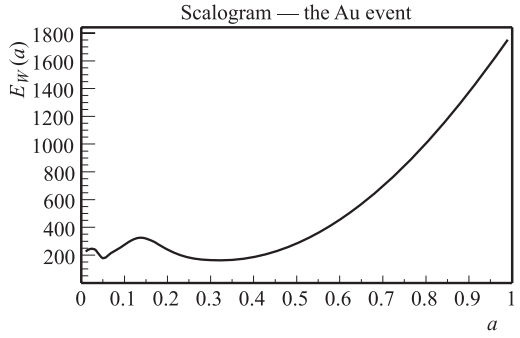

Fig. 6. Scalogram for the previous event. Its local maximums indicate relevant scales

2. the projectile fragmentation region at high pseudorapidities, 3. the central region at medium pseudorapidities.

When combining many plots like those in Fig. 4, three-dimensional graph can be constructed illustrating the dependence of $W_\Psi(a,b)$ coefficients on pseudorapidity b and scale a. The example for the random Au event with multiplicity ≈ 100 is presented in Fig. 5. The local maximums in the wavelet spectrum are

interpreted as the preferred pseudorapidities of particle groups seen at the characteristic scales. When moving along the scale axis, the evolution of clusterization of particles can be examined.

Figure 5 also indicates the most dominant scales since the maximums corresponding to groups of particles are visible mainly in the scale range from 0.05 to 0.5. This can be verified by constructing the so-called scalogram defined as: $E_W(a) = \int W_\Psi(a,b)^2 db$. The example of scalogram for the previous event is shown in Fig. 6. Its local maximums indicate relevant scales.

The Au scalogram hints at the existence of only one relevant scale since the maximum at the smallest scales (< 0.05) is trivial as it is attributed to statistical fluctuations when only individual or small groups of particles are observed.

4. STUDY OF EXTREMUM POINTS IN THE WAVELET SPECTRA

The previous example proves the ability of the wavelet method to detect the characteristic scales and pseudorapidities (in one single event). In some other event probably different prevailing scales and preferred pseudorapidity would be found. The question can be raised if there are any typical scales and pseudorapidities occurring systematically in many events or they appear only randomly. It can be revealed by investigating extremum points in the wavelet spectra of large sample of events, yet still on the event-by-event basis.

The motivation behind is that the ring-like structures are assumed to appear at similar scales and probably at a few distinguished (preferred) pseudorapidities in all events which would be manifested by local maximums in the wavelet spectra $W_\Psi(a,b)$ of large sample of events.

Figure 7 presents the distribution of maximum points collected from the scalograms of all events. Some characteristic scales are indicated at $a \approx 0.1$ and

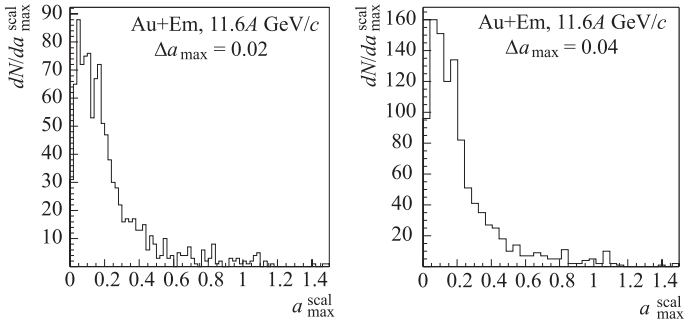

Fig. 7. Distribution of maximum points found in the scalograms of Au events

$a \approx 0.2$ but due to the low statistics it is difficult to distinguish the signals (if any) from background. Therefore, the spectra in Fig. 7 are found to be inconclusive.

Figure 8 shows how many prevailing scales usually occur in the studied events. The spectra point at the existence of one or two characteristic scales, since one maximum related to the statistical fluctuations at the smallest scales is present in the most events. The possible interpretation is that the two classes of

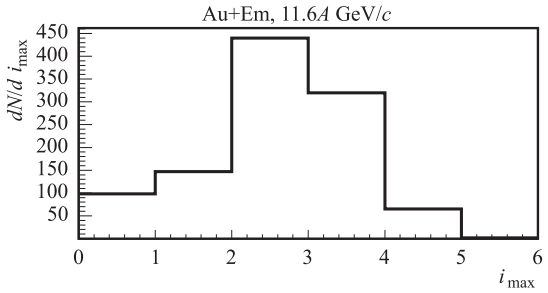

Fig. 8. Number of maximums found in the scalograms of Au events

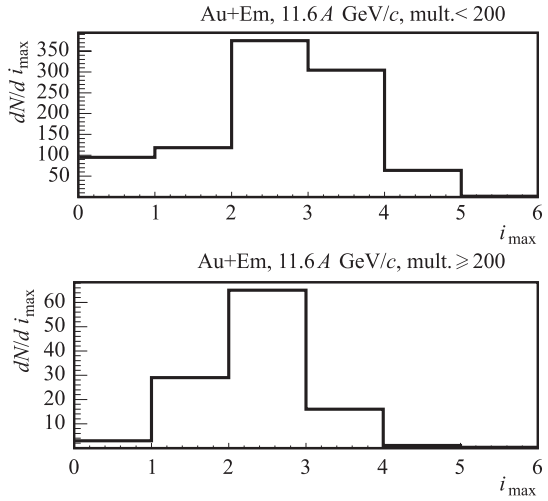

Fig. 9. Number of maximums found in Au+Em scalograms for the low and the high multiplicity events

events are identified. The events without any prevailing scales correspond mainly to unstable low multiplicity events where some scalogram maximums would be possibly found outside the examined scale range, i. e., at either extremely large or

extremely small scales, where some reasonable or valuable physical interpretation is rather unlikely.

The brief investigation of the multiplicity dependence presented in Fig. 9 implies that the high multiplicities events have only one typical scale.

After the completion of the analysis of scalograms, we can turn our attention to the three-dimensional wavelet spectra. Figure 10 displays the distribution of the number of local maximums $W_\Psi(a_{\max}, b_{\max})$ localized in the wavelet pseudo-

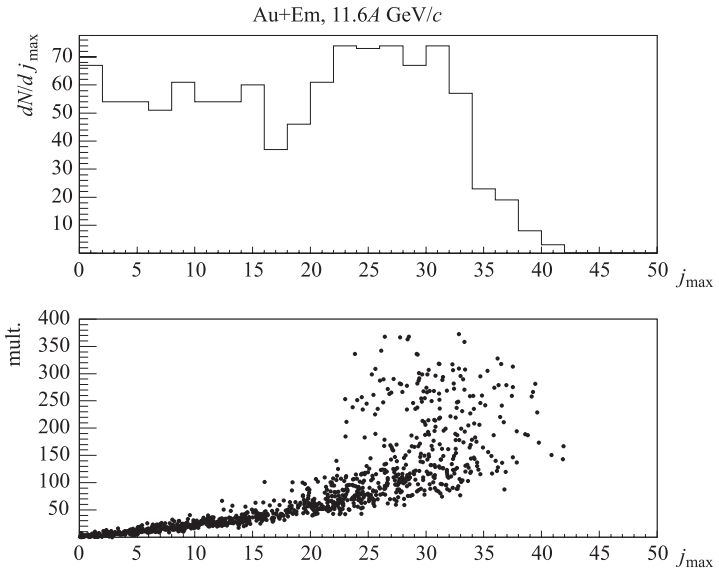

Fig. 10. Number of maximums found in the wavelet spectra $W_\Psi(a, b)$ of Au+Em events in the range of all the examined scales and its dependence on the multiplicities

rapidity spectra of Au+Em events along with the dependence on the multiplicities of s-particles. As already mentioned, each maximum can be associated with particle group moving at some pseudorapidity b. The discontinuity in the upper plot at $j_{\max} \approx 17$ dividing the $j_{\max}$ distribution to two parts is obviously related to the multiplicities which follow from the spectrum mult. vs $j_{\max}$ in the lower plot. The two modes are obvious:

• The low multiplicity mode where $j_{\max}$ rises approximately proportionally with the multiplicities. In this region only small particle groups are observed and it is dominated by statistical fluctuations.

• The stabilized high multiplicity mode where statistical fluctuations are suppressed and «real» collective particle flows are uncovered. Their number does not depend on the multiplicities anymore and seems slowly converging to a certain

value. But this speculation cannot be verified because of the absence of events with the multiplicities higher than 400.

The boundary between the two regions lies at the multiplicities about 150.

The wavelet analysis of pseudorapidity spectra is accomplished by the study of $b_{\max}$ distributions, i. e., the pseudorapidities where the wavelet maximums $W_\Psi(a_{\max}, b_{\max})$ were found. The $b_{\max}$ spectra are displayed in Fig. 11.

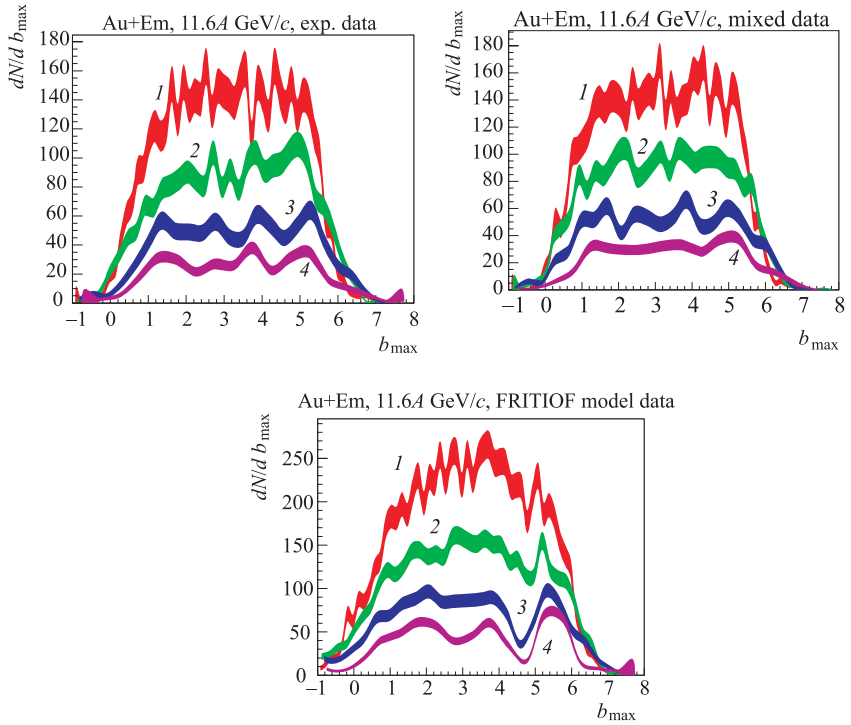

Fig. 11. The $b_{\max}$ spectra of the experimental, mixed and FRITIOF model Au+Em events seen in the four scale bands: 1) $0.05 < a_{\max} \leqslant 0.1$, 2) $0.1 < a_{\max} \leqslant 0.2$, 3) $0.2 < a_{\max} \leqslant 0.3$, 4) $0.3 < a_{\max} \leqslant 0.45$.

Local maximums in $b_{\max}$ distributions referred to as irregularities suggest the preferred pseudorapidities of particle groups. To examine their scale dependence, the $b_{\max}$ spectra are plotted at the four different scale bands*. In addition, the $b_{\max}$ distributions are compared with their analogues obtained from the FRITIOF

*The $b_{\max}$ distributions in some scale bands are multiplied by arbitrary normalization factors to avoid their mutual overlap, i. e., mainly the shapes of the distributions are relevant.

model and the mixed data**. Irregularities in the $b_{\max}$ spectra indicating the existence of collective particle flows are visible in all the investigated scale bands though some of them are insignificant from statistical point of view. Yet, some irregularities seem stable which is supported by their repeated occurrence in the mixed data.

The FRITIOF model describes the coarse features of the $b_{\max}$ spectra but fails to describe some details at all the studied scales. The differences are in the global shapes of the distributions as well as in the shapes of the irregularities. In addition, it seems that some irregularities in the experimental data have no counterparts in the model data.

The crucial question still remains: can the irregularities found in the wavelet pseudorapidity spectra be related to the ring-like structures? In order to find the answer it is necessary to proceed to analysis of azimuthal distributions.

5. STUDY OF AZIMUTHAL DISTRIBUTIONS

The existence of the preferred emission polar angles in the wavelet spectra of secondary particles produced in the Au+Em interactions does not provide sufficient evidence for the existence of ring-like structures. The effect might be alternatively clarified by an occurrence of so-called jet-like structures which is a rather cautious term denoting groups of particles correlated in both pseudorapidity and azimuth, not necessarily jets. It is inevitable to investigate if the particles contributing to the irregularities in the pseudorapidity spectra are distributed uniformly over all azimuthal angles.

Basic strategic plan can be described in a few items:

• to divide the 2π azimuthal range into 12 (or 6) uniform azimuthal sectors;

• to perform the wavelet analysis independently in all azimuthal sectors;

• to combine the maximums $W_\Psi(a_{\max}, b_{\max})$ found in different azimuthal sectors but in the same pseudorapidity bins, in order to construct the ring structures candidates;

• to study the candidates through the behaviour of variable $n_{\max}$ which is defined as the number of maximums $W_\Psi(a_{\max}, b_{\max})$ found in narrow range of pseudorapidities and scales in all 12 (or 6) azimuthal sectors (see Fig. 12).

A large value of $n_{\max}$ observed at a certain pseudorapidity could hint at the presence of ring-like structure while a small $n_{\max}$ value can be explained by a random combination of either statistical or non-statistical fluctuations of jet-like nature.

**The mixed events comprise of tracks from the experimental events with close multiplicities in order to preserve the structure of events.

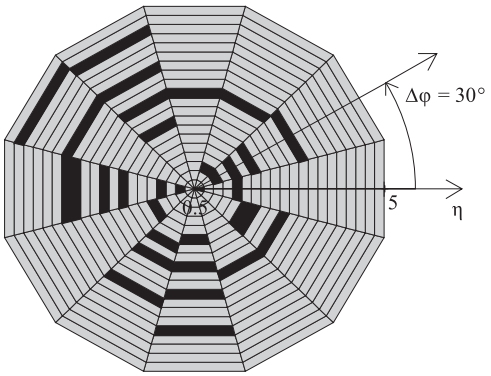

Fig. 12. An example of the target diagram for the random large multiplicity Au+Em event (mult. > 300) indicating the distribution of maximums $W_\Psi(a_{\max}, b_{\max})$ in azimuthal plane at scales $0.1 < a < 0.2$. The black slabs indicate η bins where maximums $W_\Psi(a_{\max}, b_{\max})$ are located

5.1. Monte Carlo tests. The developed ring-like structures seeking algorithm is verified on the MC simulated data as well as the background and the mixed data samples in order to test and evaluate its efficiency.

First, 600 events are generated containing 3 ring structures with the following properties:

• pseudorapidity distribution of each ring is Gaussian and centered at pseudorapidities 2, 3 and 4 with standard deviations $\sigma = 0.1, 0.2$ and 0.3, respectively;

• uniform azimuthal distribution;

• the multiplicity of particles in all the three rings is always the same and rises gradually from 1 in the first ten events to 60 in the last ten events (to test how the efficiency of the method depends on the intensity of signals).

The widths and positions of the simulated signals follow from the experimental data. The effect is most likely in the central pseudorapidity region: $1 \leqslant \eta \leqslant 5$, and roughly in the scale interval $0.05 \leqslant a \leqslant 0.5$ which is documented in the previous figures.

Then, the simulated ring structures are embedded to the experimental background. The background is built up from all gold events which are mixed regardless of their multiplicities in order to suppress particle correlations as much as possible, i. e., the mixed file comprises identical number of events with the same multiplicities as those in the experimental file, only the tracks are shuffled.

However, for the purposes of this analysis only the mixed events with the multiplicities of s-particles above 200 are used which is the same selection criterion as is applied to the real data. This selection is introduced mainly to ensure

that a sufficient number of tracks will fall to each azimuthal sector. The additional reason follows from Fig. 10 where the change of event structure is observed for events with multiplicities above ≈ 150.

Usually, the spectra η vs $n_{\max}$ in the different scale bands are surveyed in order to study the dependence of $n_{\max}$ on pseudorapidity and scale as well. That could show if the ring-structures candidates tend to appear randomly or at some distinguished pseudorapidities. In the experimental data (which is studied in the next section) these pseudorapidities should coincide with the previously found pseudorapidity irregularities presented in Fig. 11.

Each point in the η vs $n_{\max}$ plots represents a ring-structure candidate stretched over the number $n_{\max}$ of azimuthal sectors.

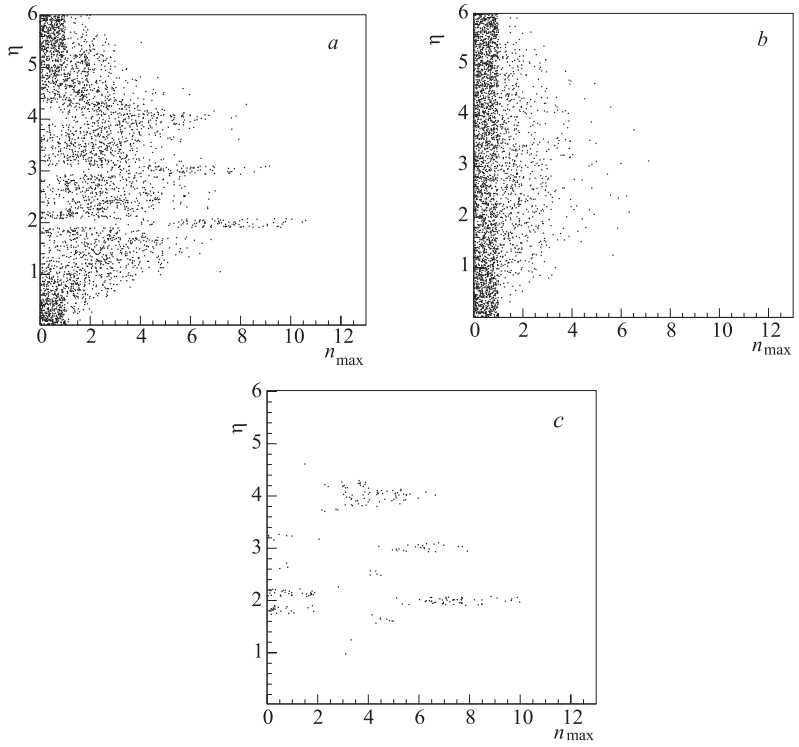

Fig. 13. Distribution of η vs $n_{\max}$ of the mixed+simulated (a) and the mixed events (b) for the scale band $0.05 < a_{\max} \leqslant 0.15$. The multiplicities of particles of the embedded rings in (a) are: $25 \leqslant \mathrm{mult.} \leqslant 35$; ($c$) shows the result after the subtraction of both previous spectra

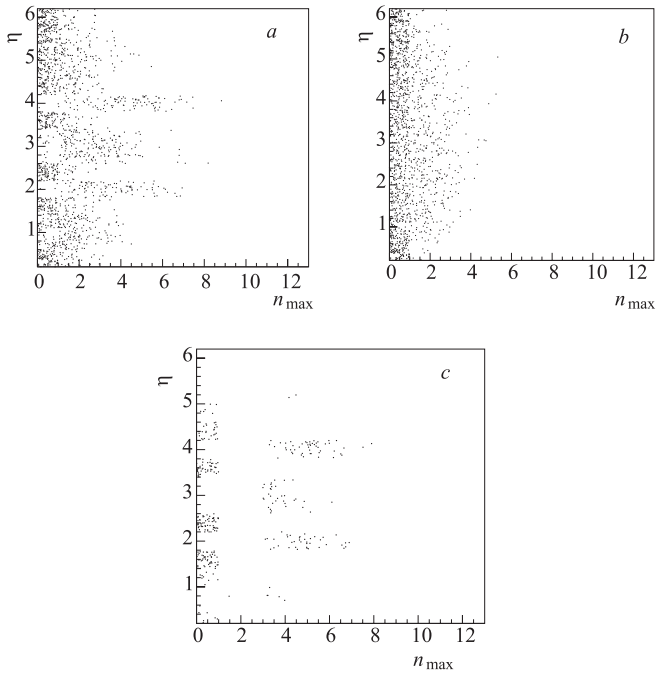

Fig. 14. Distribution of η vs $n_{\max}$ of the mixed+simulated (a) and the mixed events (b) for the scale band $0.2 < a_{\max} \leqslant 0.35$. The multiplicities of particles of the embedded rings in (a) are: $25 \leqslant \mathrm{mult.} \leqslant 35$; ($c$) shows the result after the subtraction of both previous spectra

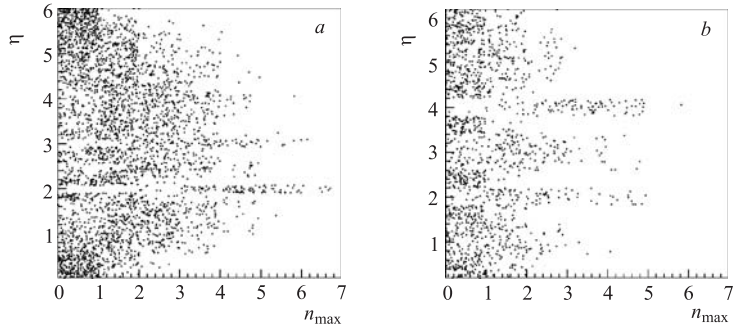

Fig. 15. Distribution of η vs $n_{\max}$ of the mixed+simulated events for the scale bands $0.05 < a_{\max} \leqslant 0.15$ (a) and $0.2 < a_{\max} \leqslant 0.35$ (b) when only six uniform azimuthal sectors are used. The multiplicities of particles of the embedded rings vary from 25 to 35

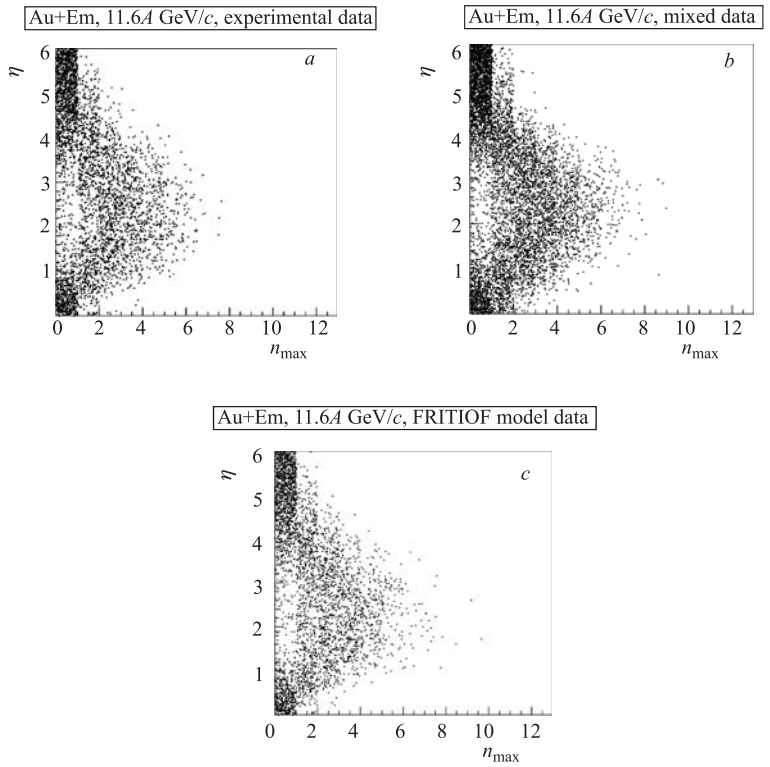

Fig. 16. Distribution of η vs $n_{\max}$ in the scale band $0.05 < a_{\max} \leqslant 0.15$ ($a \approx 0.1$) for the Au+Em experimental (a), mixed (b) and FRITIOF model (c) events with multiplicities above 200

Figure 13 shows the η vs $n_{\max}$ distribution of the background+simulated events, the background events and the result after their subtraction, respectively. The effect is incorporated in all the background+simulated events, i. e., the contribution of events containing signal is 100%. The multiplicities of particles of the embedded rings are about 30 and $a_{\max}$ scales lie in the interval $0.05 < a_{\max} \leqslant 0.15$.

In the scale band $0.05 < a_{\max} \leqslant 0.15$ we assume to detect mainly the rings with $\sigma \approx 0.1$. The ring-like structures jutting out of background at $\eta = 2$ in Fig. 13, (a) are clearly visible. Even the other two ring structures at $\eta = 3$ and $\eta = 4$ are distinguishable though their optimum resolution is due to their larger widths reached at larger scales. Their remnants in Fig. 13, (a) result from smearing in scale space which in general depends on the multiplicities of ring

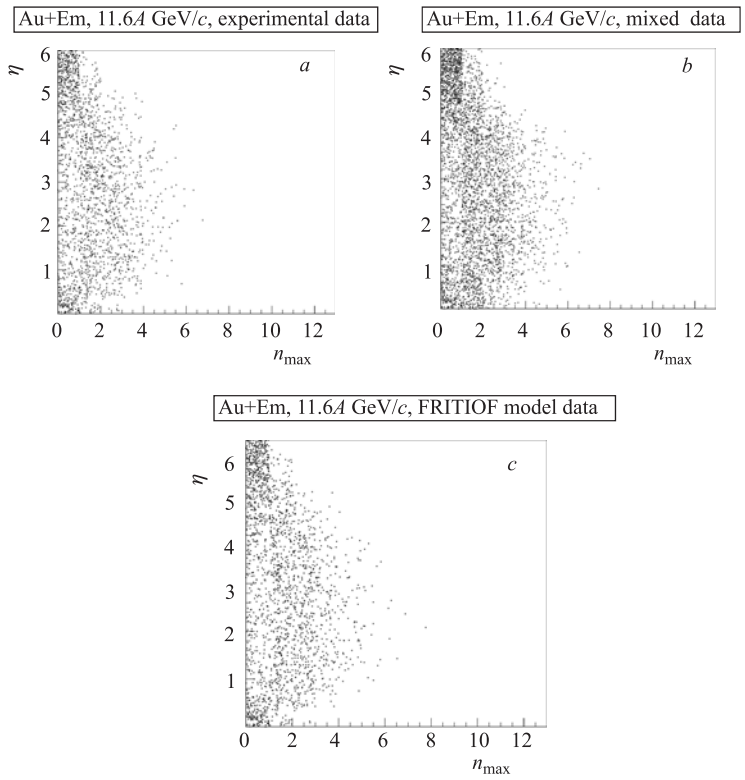

Fig. 17. Distribution of η vs $n_{\max}$ in the scale band $0.15 < a_{\max} \leqslant 0.3$ ($a \approx 0.2$) for the Au+Em experimental (a), mixed (b) and FRITIOF model (c) events with multiplicities above 200

structures, the background properties and the efficiency of the wavelet based algorithm. Overflows between different scale bands can be reduced by enlarging their widths. On the other hand, too broad scale bands would lead to undesired mixing of different scales. Therefore, the scale bands employed in our analysis are chosen as a reasonable compromise estimated by Monte Carlo simulations.

Figure 14 shows the η vs $n_{\max}$ distribution of the background+simulated events, the background events and the result after their subtraction, respectively. The analyzed multiplicities are the same as in Fig. 13, but now the scale band $0.2 < a_{\max} \leqslant 0.35$ is chosen to achieve the best resolution for ring structures of typical width $\sigma \approx 0.3$. As expected, the broadest ring at $\eta = 4$ is the best visible though the contrast when compared to background is less evident. Also, the difference between the ring at $\eta = 4$ and the narrower rings at $\eta = 2$ and

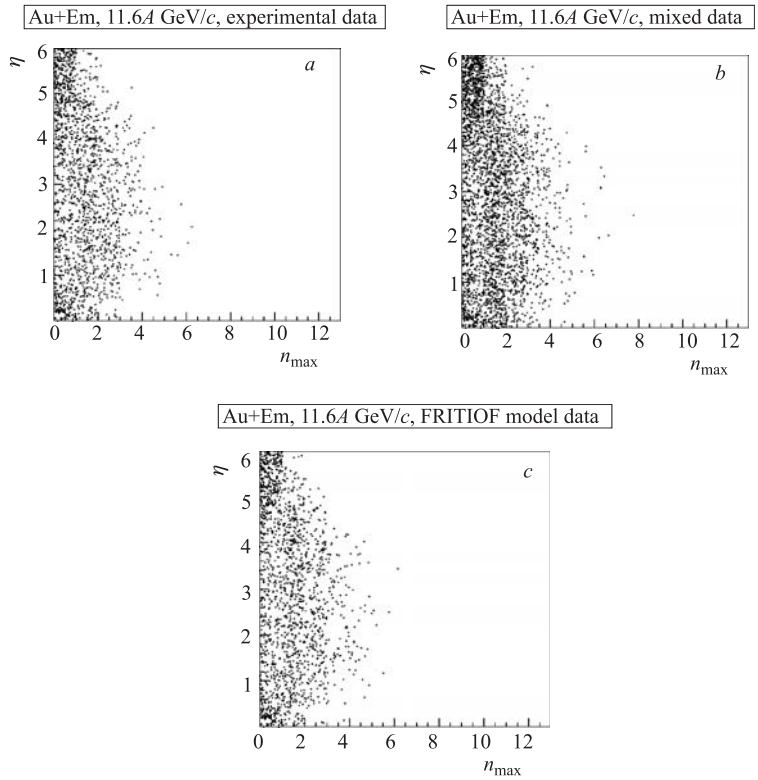

Fig. 18. Distribution of η vs $n_{\max}$ in the scale band $0.2 < a_{\max} \leqslant 0.35$ ($a \approx 0.3$) for the Au+Em experimental (a), mixed (b) and FRITIOF model (c) events with multiplicities above 200

$\eta = 3$ is less pronounced. This can be explained by lower η density of particles in the wide ring structures which are therefore worse defined and consequently more smeared not only in η but in the scale space as well.

Figure 15 presents the plots analogous to Figs. 13, (a) and 14, (a) but for the total number of 6 azimuthal sectors only while the previous figures are produced when using totally 12 azimuthal sectors. It seems the potential space for the signals to run out from the background is reduced, especially in Fig. 15, (a), which could make their detection more difficult.

The spectra similar to those in the displayed examples are created for the other intervals of scales and multiplicities of particles of the embedded rings but it is barely possible to present them all.

5.2. Results. Since the previous plots prove the ability of the method to detect the ring-like structures in the expected range of scales, we can finally proceed to

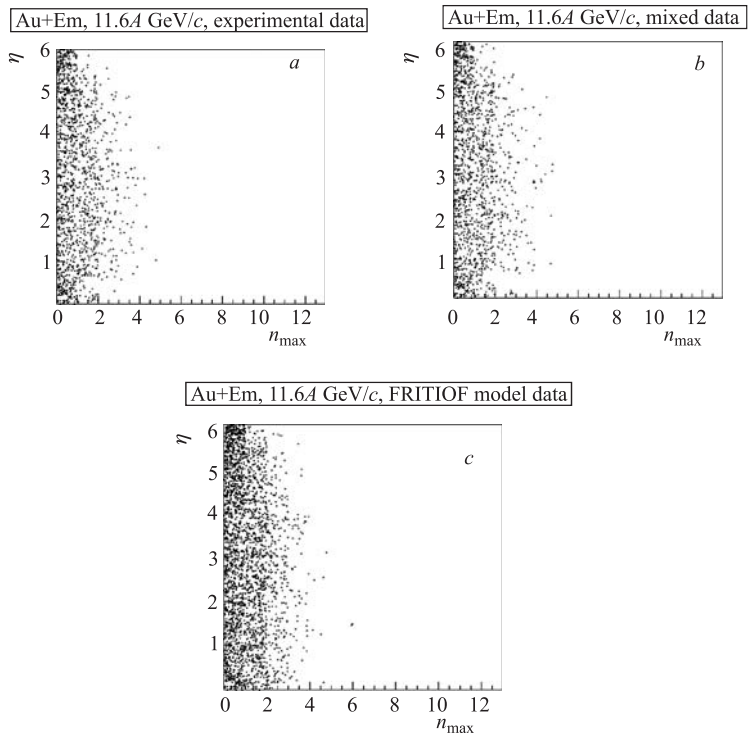

Fig. 19. Distribution of η vs $n_{\max}$ in the scale band $0.3 < a_{\max} \leqslant 0.45$ $(a \approx 0.4)$ for the Au+Em experimental (a), mixed (b) and FRITIOF model (c) events with multiplicities above 200

the experimental data. The η vs $n_{\max}$ plots are shown for the analysis carried out in 12 azimuthal sectors but similar results are obtained for only 6 azimuthal sectors as well. The experimental η vs $n_{\max}$ spectra are always compared with their FRITIOF model or the mixed data counterparts where no ring-like structures are present.

The η vs $n_{\max}$ plots at the four different scale bands are presented in Figs. 16, 17, 18 and 19. The experimental η vs $n_{\max}$ plots do not exhibit any extraordinary behaviour that could suggest the presence of ring-like structures since no conspicuous clusters of points sufficiently projecting from the background to the region of large $n_{\max}$ are observed. The conclusion is valid for all the investigated scales. A few anomalous points emerging from the background in the experimental spectra do not provide sufficient evidence because they use to appear in the model and the mixed data distributions as well. Moreover, they tend

to occur at random pseudorapidities and do not concentrate on a few preferred pseudorapidities.

To conclude, the η vs $n_{\max}$ plots do not prove the existence of the ring-like structures in the Au+Em data.

SUMMARY

• Angular spectra of the relativistic secondary particles produced in Au+Em nuclear collisions at 11.6A GeV/c are analyzed by the method of continuous wavelet transform.

• The so-called irregularities are revealed in the wavelet pseudorapidity spectra in the scale pseudorapidity region up to 0.5. These irregularities are interpreted as the preferred emission polar angles of groups of particles.

• The present study of the azimuthal distributions of the above-mentioned pseudorapidity irregularities suggests they are not related to the ring-like structures with the properties defined in Abstract or at the end of Chapter 1.

Acknowledgements. This work was supported by Slovak Research and Development Agency under the contract No. APVT-20-011704.

REFERENCES

1. *Dremin I. M.* // Pisma v ZhETF. 1979. V. 30. P. 152.
2. *Dremin I. M.* // Yad. Fiz. 1981. V. 33. P. 1357.
3. *Glassgold A. E., Heckrotte W., Watson K. M.* // Ann. Phys. 1959. V. 6. P. 1.
4. *Casalderey-Solana J., Shuryak E. V., Teaney D.* // J. Phys. Conf. Ser. 2005. V. 27. P. 22.
5. *Adamovich M. I. et al.* // Eur. Phys. J. 1999. V. 5. P. 429.
6. *Dremin I. M., Astafyeva N. M., Kotelnikov K. A.* // Mod. Phys. Lett. A. 1997. V. 12. P. 1185.
7. *Uzhinsky V. et al.* // JINR, P1-2001-119. Dubna, 2001.

Received on January 15, 2007.

Редактор *В. В. Рудниченко*

Подписано в печать 14.03.2007.
Формат 60 × 90/16. Бумага офсетная. Печать офсетная.
Усл. печ. л. 1,37. Уч.-изд. л. 1,94. Тираж 365 экз. Заказ № 55693.

Издательский отдел Объединенного института ядерных исследований
141980, г. Дубна, Московская обл., ул. Жолио-Кюри, 6.
E-mail: publish@jinr.ru
www.jinr.ru/publish/